Geophysical Research Letters

Correspondence to:
Y. Zheng,
zhengyoutong@gmail.com

A More General Paradigm for Understanding the Decoupling of Stratocumulus-Topped Boundary Layers: The Importance of Horizontal Temperature Advection

Youtong Zheng[1] iD, **Daniel Rosenfeld[2]** iD, **and Zhanqing Li[1]** iD

[1]Earth System Science Interdisciplinary Center, University of Maryland, College Park, MD, USA, [2]Institute of Earth Science, Hebrew University of Jerusalem, Jerusalem, Israel

Abstract Most prior studies on decoupling of a stratocumulus-topped boundary layer (STBL) are focused on subtropics where cold air advection with moderate strength is dominant. This study expands across a wider spectrum of temperature advection spanning from moderately strong warm air advection to extremely strong cold air advection. A STBL undergoing warm advection is found to be more mixed than a STBL undergoing cold advection. This finding is consistent with the cold advection facilitating turbulent mixing in the boundary layer. When cold advection becomes sufficiently strong (<-5 K/day), the STBL becomes more stably stratified again because of emergence of the cumulus-coupled STBL regime induced by the "deepening-warming" mechanism. Such a "deepening-warming" induced STBL decoupling, however, is still much weaker than that caused by warm advection flows (even weak ones), suggesting that the direction and strength of temperature advection must be considered for any STBL decoupling studies.

1. Introduction

Marine stratocumulus clouds are important to the energy budget of the planet (Hartmann et al., 1992). They are strongly coupled with planetary boundary layer processes, forming stratocumulus-topped boundary layers (STBL), a system with complex feedbacks between surface fluxes, convection, radiation, entrainment, and cloud physics (Wood, 2012). STBL properties are considerably regulated by the extent to which the STBL decouples from the underlying sea surface fluxes (Bretherton, 1997; Jones et al., 2011; Wood, 2012; Zheng et al., 2016). The most commonly used definition of the STBL decoupling is based on the thermodynamic stratification of a STBL (Stephen Nicholls, 1984): A STBL is defined as decoupled if moist-conserved variables (e.g., liquid water potential temperature or total liquid water content) cease to be well mixed in the boundary layer.

Previous studies of STBL decoupling are mostly limited to subtropical oceans where cold air advection is prevalent (Jones et al., 2011; Nicholls & Leighton, 1986; Stephen Nicholls, 1984; Stevens et al., 1998; Wood & Bretherton, 2004; Zheng et al., 2018a). The subtropics are of particular interest because of the climatologically important subtropical stratocumulus-to-cumulus transitions, during which the STBL stratification (i.e., decoupling) is a key intermediate step. The stably stratified STBLs in the subtropical downstream are often "cumulus-coupled" (Bretherton, 1997; Miller & Albrecht, 1995). The reason is that cold advection facilitates the buildup of mean flow potential energy of the lower atmosphere that sustains a conditionally unstable subcloud layer, allowing cumulus convection to be invigorated. Is the cumulus-coupled STBL coupled or decoupled? Debates abound (e.g., Miller & Albrecht, 1995; Stevens et al., 1998; Zheng et al., 2018b). Instead of setting a clear-cut distinction between decoupled and coupled STBLs, this study treats the "decoupling" as a spectrum in which the well-mixed STBL corresponds to the most coupled extreme and the cumulus-coupled STBL situates somewhere in the middle where the boundary layer is stably stratified, but not stable enough to shut off the cumulus convection. The most decoupled extreme corresponds to highly stratified STBLs without cumulus coupling. Recently, Zheng and Li (2019) documented that such strongly decoupled STBLs are most likely to occur in warm advection conditions in which shallow cumulus convection is suppressed due to the high stability in the subcloud layer. This new finding suggests that it is critically important to consider the strength and direction of low-level temperature advection if one wants to understand the STBL coupling state across the whole spectrum ranging from well-mixed STBLs, to

weakly stratified STBLs with cumulus coupling, to strongly stratified STBLs without cumulus coupling. This motivates the current study. Here, we advocate for using the low-level temperature advection as a key environmental variable to understand the STBL decoupling. This idea represents a more general paradigm than the conventional view that is largely confined to cold air advection conditions.

There are plenty of prior studies that attempt to link the strength and direction of temperature advection with boundary layer cloud properties (Albrecht et al., 1988; Bretherton et al., 1995; George & Wood, 2010; Klein, 1997; Klein et al., 1995; Norris & Iacobellis, 2005; Norris & Klein, 2000; Wall et al., 2017; Wylie et al., 1989; Xu et al., 2005). Their analyses are based on either satellite data or buoy measurements. Both tools can only provide bulk properties of clouds (e.g., cloud coverage and cloud optical thickness), but not vertical details of STBLs. As a result, direct observational evidence of how STBL coupling state responds to temperature advection is lacking, although inferences are plenty (Klein, 1997; Norris & Iacobellis, 2005; Norris & Klein, 2000). In this study, we use ground observations (balloon-borne radiosonde with the aid of W-band cloud radar) to quantify the STBL thermodynamic decoupling degree over three field experiments under the aegis of Department of Energy (DOE) Atmospheric System Research (ASR) program. Oceans covered by the three field campaigns are the subtropical northeast Pacific, the Southern Oceans, and the eastern north Atlantic that straddles the boundary between the midlatitudes and the subtropics. These regions encompass a range of different large-scale dynamics so that STBLs under the influence of a wide spectrum of temperature advection can be sampled.

Data and methodology are described in the next section. Section 3 shows the results from composite analysis. Section 4 summarizes the findings.

2. Data and Methods

2.1. Ground Observations

We use ground-based observations from three U.S. Department of Energy (DOE)/Atmospheric Radiation Measurement (ARM) field campaigns: (1) The Clouds, Aerosols, and Precipitation in the Marine Boundary Layer (CAP-MBL) (Wood et al., 2015), (2) Marine ARM GPCI (Global Energy and Water Cycle Experiment [GEWEX]-Cloud System Study [GCSS]-Pacific Cross-section Intercomparison) Investigation of Clouds (MAGIC) (Lewis, 2016), and (3) Measurements of Aerosols, Radiation, and CloUds over the Southern Ocean (MARCUS) (McFarquhar et al., 2019). All of the three field campaigns are located over open oceans. They are deployed with the ARM Mobile Facility (AMF) including the balloon-borne sounding system, W-Band (95 GHz) ARM Cloud Radar (WACR), Vaisala ceilometer, and routine surface meteorological instrumentation.

2.1.1. MAGIC

MAGIC was conducted by a cargo ship carrying the AMF sailing routinely across the northeast Pacific Ocean between Los Angeles, California, and Honolulu, Hawaii. The campaign lasted for one full year from October 2012 to September 2013, but because of a 5-month dry dock, only 7-month-worth of data are available. A uniqueness of MAGIC lies in the transect of a climatologically important cloud regime transition: from the upstream semi-permanent stratocumulus decks to the downstream broken trade cumulus. The STBLs are under the continuous influence of large-scale subsidence from the subtropical high. The trade winds tend to mobilize the STBLs equatorward so that this region is dominated by cold air advection.

2.1.2. CAP-MBL

The CAP-MBL is a 19-month field study on Graciosa Island, Azores, in the northeast Atlantic. Unlike the MAGIC region where the synoptic forcing is relatively stable with time, the Graciosa Island is under the influence of a much wider range of synoptic scale meteorological conditions. Because the Graciosa is located near the boundary between the subtropics and the mid-latitudes, it is subject to the impacts of not only the subtropics-characterized trade wind system but also the midlatitude cyclonic systems. Such a wide range of meteorological conditions allows samplings of STBLs under the influence of different directions and strengths of thermal advection.

2.1.3. MARCUS

The MARCUS was conducted over the Southern Ocean on an Australian vessel equipped with the AMF that routinely traveled between Hobart (43°S, 147°E), Australia, and several Antarctic coast stations from October 2017 to April 2018. As the stormiest region on Earth, the Southern Ocean is very rich in midlatitude cyclones

and the associated frontal systems. Because of its remoteness from anthropogenic regions, the Southern Ocean is considered as one of the most pristine regions on Earth.

2.2. Satellite and Reanalysis Data

We use the geostationary satellite data from the 15th Geostationary Operational Environmental Satellite (GOES-15), Meteosat Second Generation satellite (Meteosat-9), and Himawari-8, to obtain low-cloud fraction for MAGIC, CAP-MBL, and MARCUS, respectively. The data are obtained from the National Aeronautics and Space Administration (NASA) Langley Cloud and Radiation Research Group (http://www-angler.larc.nasa.gov). The European Centre for Medium-Range Weather Forecasts (ECMWF) Interim reanalysis data (Berrisford et al., 2011) are used to generate synoptic meteorology. The reanalysis variables include SST, wind vectors and temperature at 900 hPa, and vertical velocity at 500 hPa.

2.3. Detection of Atmospheric Fronts

Temperature advection, if adequately strong, is associated with atmospheric fronts. The frontal lifting and the resultant kinetic impacts of synoptic dynamics complicate the analysis. Thus, it is necessary to diagnose to what extent the sampled clouds are subject to kinetic influences from atmospheric fronts. As such, an objective method for front detection is needed. In this study, we use a new front detection algorithm developed by Parfitt et al. (2017). This algorithm detects atmospheric fronts using the normalized product of the relative vorticity and horizontal temperature gradient, which is defined as the F diagnostic (see Text S1 for a description). In this study, the F diagnostic is computed using wind and temperature fields at 900 hPa from ECMWF reanalysis data. If the F is greater a certain threshold (we set it as 1), the region is considered as a frontal region.

2.4. Case Selection

We surveyed all $1.5 \times 1.5°$ satellite scenes centered on the locations of the ships or the island during the entire periods of the three experiments. Scenes with low cloud amount greater than 50% are selected, in which the low cloud pixels are defined as those with satellite-derived cloud-top height (Minnis et al., 1995) lower than 3 km. This limits our analysis to typical stratiform clouds or cumuliform clouds coexisting with partially broken stratiform anvils (e.g., open cells). Use of this criterion automatically removes shallow cumulus with cloud fraction <50%. There are two reasons for setting this criterion. First, the concept of coupling/decoupling was initially proposed, and has been subsequently used, for stratiform boundary layer clouds only. Second, as will be shown later, we need to use radiosonde data to calculate a STBL decoupling metric, which requires the identification of the inversion layer height. Stratiform clouds typically have well-defined temperature inversions that help us avoid the known problem of identification of weak inversions for cumuliform cloud regimes (Jones et al., 2011). By visual inspection of radiosonde profiles and cloud radar images, we found that the cloud fraction of 50% is a reasonable threshold, above which the identification of capping inversion layer is rather robust. Further increasing the threshold does not affect primary results, but decreases the number of samples (Figure S2). To minimize the potential influence of frontal kinetic lifting, cases with $F > 1$ were removed. This removes ~5% of the cases. The main result is not sensitive to the threshold of F (Figure S2). Based on these criteria, a total of 621 cases during CAP-MBL, 134 cases during MAGIC, and 94 cases during MARCUS are selected. The selected low-lying stratiform clouds are more likely to occur in environments with cold advection and large-scale subsidence (Figure S3), consistent with our previous knowledge (Norris & Klein, 2000). Moreover, Figure S3 shows that the majority of warm advection cases occur in CAP-MBL and MARCUS, consistent with our expectation that subtropical field campaigns (such as the MAGIC) sample limited warm advection events.

For each identified satellite scene, we use ground measurements with ±1.5 hr time window centered on the satellite sampling time. We use the nearest radiosonde data to identify the inversion layer height (z_i), which is determined as the altitude where the potential temperature inversion strength (dθ/dz) is the largest below 3.5 km. The three-point moving average smoothing was performed for the radiosonde data before the z_i identification. To guarantee that this method correctly identifies the real inversion layer capping the stratiform clouds, not other inversions that may occur in subcloud layers, we visually examine all the W-band cloud radar images (see an example in Figure S4). Surprisingly, such a simple method performs very well for nearly all the selected cases. Such a good performance may be attributed to two reasons. First, strong subcloud-layer temperature inversions are most likely to occur in STBLs in atmospheric fronts, and such cases are already

removed. Second, under warm air advection, temperature inversion may occur below stratocumulus bases (Whiteman et al., 1999), but the boundary layer turbulent mixing, either by surface wind shear or cloud-top radiative cooling, contributes to the weakening of the inversion so that the capping inversion is always stronger (see such a case in Figure S4).

To measure the decoupling degree of a STBL, we, by following Jones et al. (2011), use the decoupling metric: θ_e^{top}-θ_e^{bot}, in which the θ_e is the radiosonde-measured equivalent potential temperature and the subscripts "top" and "bot" represent the means of the top and bottom 25% of the boundary layer below the inversion, respectively. We select Jones et al.'s (2011) method because of its simplicity and straightforward physical meaning.

2.5. Backward Trajectory Analysis

To obtain the strength of the low-level thermal advection, we run the Hybrid Single Particle Lagrangian Integrated Trajectory Model (HYSPLIT) (Stein et al., 2015) on level of 500 m above the sea surface to obtain the 36-hr backward trajectory. The model is driven by the $0.5 \times 0.5°$ Global Data Assimilation meteorology data (Kanamitsu, 1989). For each trajectory we quantify the temperature advection, T_{adv}, by

$$T_{adv} = -\overline{\frac{dSST}{dt}} = \overline{-\mathbf{V_{500\ m}} . \nabla SST}$$

where the $\mathbf{V_{500\ m}}$ is the horizontal wind vector at 500 m above sea surface. The overbar does not stand for simple average of $-\frac{dSST}{dt}$, but for taking the linear least squares trend of SST along the 36-hr trajectory. A positive T_{adv} corresponds to warm air advection.

3. Results

Figure 1a shows the relationship between STBL coupling state and z_i under different external forcing of temperature advection. We pay particular attention to z_i because it is widely identified as a good predictor of STBL decoupling (Bretherton & Wyant, 1997; Wood & Bretherton, 2004; Zheng et al., 2018b; Zuidema et al., 2009). This well-known z_i-decoupling relationship can be considered as conventional knowledge, upon which the new analysis of the role of temperature advection is based. As shown in Figure 1a, a STBL becomes increasingly more decoupled as z_i deepens, consistent with conventional wisdom. This behavior is qualitatively coherent across different groups of T_{adv}. Such a result is not surprising from an energetic point of view. As the dominant driver of STBL convection, cloud-top radiative cooling (CTRC) generates turbulent kinetic energy that contributes to the buildup of mean flow potential energy, sustaining a well-mixed STBL. A deeper STBL requires more CTRC for maintaining a well-mixed state. Since the CTRC has an upper limit (Zheng et al., 2019), a deeper STBL is more likely to be stratified.

A more interesting feature in Figure 1a is a clear separation of the data points by T_{adv}: For a given z_i, a STBL is more decoupled for a greater T_{adv}. This result is consistent with the warm air advection stabilizing the air below cloud bases and suppressing the STBL turbulent mixing. Such a dependence on T_{adv} becomes less pronounced in shallower STBLs in which shallow STBLs demand less turbulent kinetic energy for sustaining well-mixed states so that the CTRC-driven convective mixing is always adequate to overcome the stabilization effect.

Figure 1b shows the relationships separately for the three field campaigns. Only CAP-MBL data encompass the full range of T_{adv}, which exhibits similar patterns with those in Figure 1a. This is as expected because CAP-MBL samples constitute a majority of the total samples. Consistent with the results from CAP-MBL, MARCUS data show that θ_e^{top}-θ_e^{bot} is systematically larger for $T_{adv} > 0$ K/day than those with T_{adv} between −5 and 0 K/day, but their differences are markedly smaller than in CAP-MBL in particular for $z_i > 2$ km. We do not find a physical explanation for this regional difference. Given that MARCUS samples include mixed-phase clouds in particular in deep STBLs, investigating the influence of cloud phase on STBL decoupling may be a promising approach to answer this question, which we leave for future work. For MAGIC, all the cases have T_{adv} between −5 and 0 K/day. Overall, despite the regional difference in the degree with
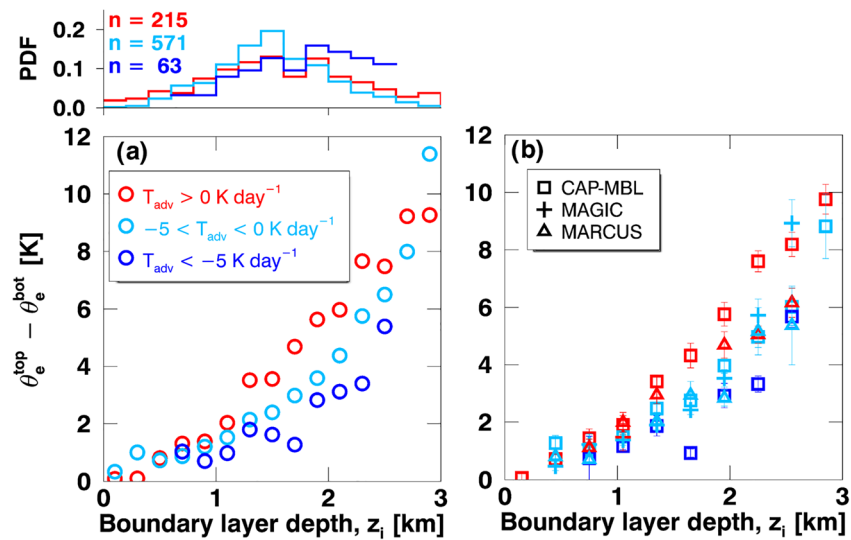
Figure 1. Radiosonde-measured θ_e^{top}-θ_e^{bot} versus the z_i for $T_{adv} > 0$ K day^{-1}, $-5 < T_{adv} < 0$ K day^{-1}, and $T_{adv} < -5$ K day^{-1} in all the samples (a) and in different field campaigns (b). In (a), each point represents an average of a 0.2-km bin of z_i, and the number of samples in each bin is plotted in the upper plot. In (b), the bin size increases to 0.3-km to include more samples. Error bars represent the standard errors of mean. Bins with less than three samples are not shown. Note that the error bars simply represent the statistical difference of samples between bins. They do not capture the uncertainties due to measurement error or the possible sampling error for the bins with scarce samples.

which θ_e^{top}-θ_e^{bot} changes with the T_{adv}, the conclusion of warm advection strengthening the decoupling holds.

Figure 2a shows the θ_e^{top}-θ_e^{bot} versus T_{adv} during the three field campaigns. For $T_{adv} > -5$ K day^{-1}, the decoupling degree increases with increasing T_{adv}, which is consistent with the result from Figure 1. The positive dependence of θ_e^{top}-θ_e^{bot} on T_{adv}, however, shifts to weakly negative for $T_{adv} < -5$ K day^{-1} (gray shaded region). This seems to contradict with the result from Figure 1 in which θ_e^{top}-θ_e^{bot} increases with T_{adv}. This apparent contradiction can be explained by the changes in z_i. Figure 2b shows the variation of z_i with T_{adv}. For $T_{adv} < -5$ K day^{-1}, there is an overall increasing trend of z_i as cold advection becomes stronger (decrease in T_{adv}), which causes an increase in θ_e^{top}-θ_e^{bot}. For $T_{adv} > -5$ K day^{-1}, the dependence of z_i on T_{adv} presents mixed results that differ between field campaigns and different ranges of T_{adv} (see Appendix A for discussions). This causes an overall weak z_i response to T_{adv}, leaving a relatively clear signal of T_{adv} influence on STBL decoupling.

What causes such increases in both z_i and decoupling degree as cold advection strengthens? Is it just a random perturbation of z_i (given the relatively smaller number of samples) or is there any physical mechanism driving a systematically deeper and more decoupled STBLs? We favor the latter. Such a preference is motivated by the common occurrence of open-cellular STBLs during cold-air outbreaks (McCoy et al., 2017; Muhlbauer et al., 2014). From a parcel-following perspective, an extremely strong cold air advection can be considered as a cold-air outbreak event. A fast warming of the underlying sea surface causes a STBL to deepen rapidly, forming a cumulus-coupled STBL, a mechanism commonly known as "deepening-warming" decoupling (Bretherton & Wyant, 1997). The deepening can be so rapid that the initially well-mixed state sustains only for a short period of time, leaving the STBL deep and cumulus-coupled for the rest of its lifetime. As a result, deeper and cumulus-coupled STBLs are more likely to be sampled under strong cold air advection.

This argument can be supported by two pieces of evidence. First, there is a significant increase in the skewness of liquid water path (LWP) as cold advection strengthens for $T_{adv} < -5$ K day^{-1} (Figure 2c). The LWP field is obtained from geostationary satellite data over $2 \times 2°$ domain centered on the locations of the observation sites. Higher LWP skewness is a good indicator of the occurrence of cumulus-coupled STBLs (Zheng et al., 2018a). Second, the composite mean meteorological field for STBLs with $T_{adv} < -5$ K day^{-1} (Figure S6)

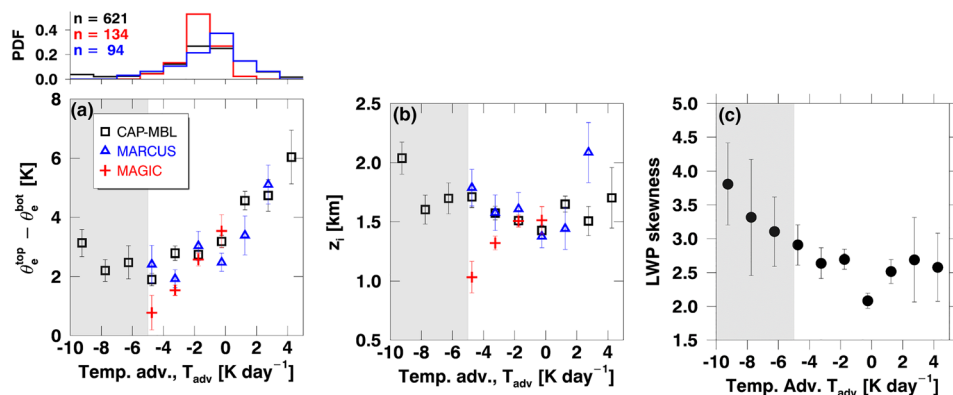**Figure 2.** Variations of radiosonde-measured θ_e^{top}-θ_e^{bot} (a), z_i (b), and satellite-retrieved LWP skewness of $2° \times 2°$ domains (c) with T_{adv}. The gray shading marks the segment with $T_{adv} < -5$ K day^{-1}. In (c), data from the three campaigns were combined to compensate for the loss of samples due to satellite-retrieved LWP being available only during daytime.

suggests that these STBLs occur just behind cold fronts, a classical synoptic configuration for open-cellular stratocumulus during cold-air outbreaks (Agee, 1987; Fletcher et al., 2016; McCoy et al., 2017).

To offer theoretical support to the argument, we use a mixed-layer model of STBL. The model formulation and the boundary and initial forcing are the same as those used in (Bretherton & Wyant, 1997) (see Text S2 for detail). An advantage of this mixed-layer model is its ability to predict the occurrence of decoupling via the buoyancy integral ratio (BIR), defined as $-\dfrac{\int_0^{z_i} F_B \mathscr{H}(-F_B)dz}{\int_0^{z_i} F_B \mathscr{H}(F_B)dz}$, in which the F_B is the buoyancy fluxes and the $\mathscr{H}$ is the Heaviside function. The physical meaning of BIR is the vertical integral of the negative buoyancy flux (typically occurs below the cloud base) divided by the vertical integral of the positive buoyancy flux across the STBL. If BIR exceeds 0.15, a STBL is considered decoupled (cessation of well-mixed state), and the mixed-layer model ceases to be valid. To examine how faster a STBL decoupling occurs under different strength of T_{adv}, we run the model in T_{adv} of -5 and -10 K day^{-1}, which are shown in Figures 3a and 3b, respectively. The STBL in T_{adv} of -10 K day^{-1} becomes decoupled ~ 15 hr earlier than T_{adv} of -5 K day^{-1}. As a thought experiment, we can imagine these two STBLs being advected toward an observation site and being sampled at $t = 36$ hr (this is the time length of backward trajectory we use for computing the T_{adv}). At the time of sampling, the STBL for T_{adv} of -5 K day^{-1} still remains well mixed whereas the STBL for T_{adv} of -10 K day^{-1} is already decoupled with higher z_i. This is, of course, a very idealized conceptualization. In the real world, sampled STBLs can be in any stage of their life cycles. Statistically speaking, STBLs under very strong cold advection remain well mixed for a considerably shorter period of time than relatively weaker cold advection (Figure 3), so that the sampled STBLs in strong cold air advection are more likely to be deeper and decoupled.
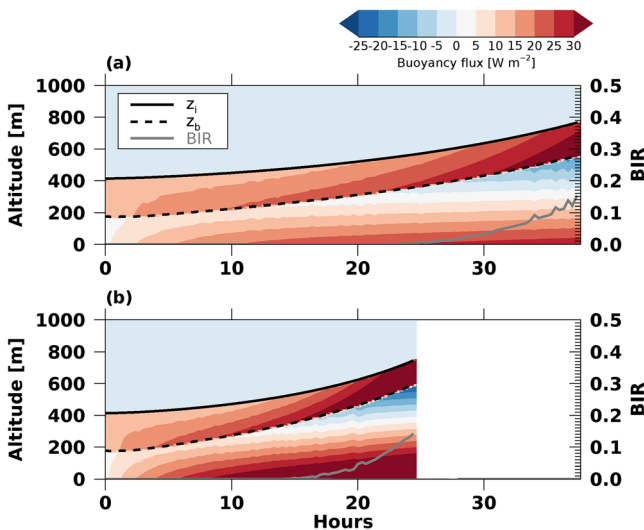

Figure 3. Height-time plots of buoyancy fluxes simulated by the mixed-layer model in temperature advections of -5 K day^{-1} (a) and -10 K day^{-1} (b). The z_b is the cloud-base height.

4. Discussion and Conclusions

This study demonstrates the importance of horizontal low-level temperature advection in understanding the decoupling of a stratocumulus-topped boundary layers (STBL). Here the decoupling is defined as the degree of thermodynamic stratification of a STBL. Unlike previous studies that investigate STBL decoupling in limited ranges of temperature advection (e.g., subtropical air flowing equatorward, warm air in warm sectors of midlatitude cyclones advected over colder water, and cold air outbreaks), this study examines the whole spectrum of temperature
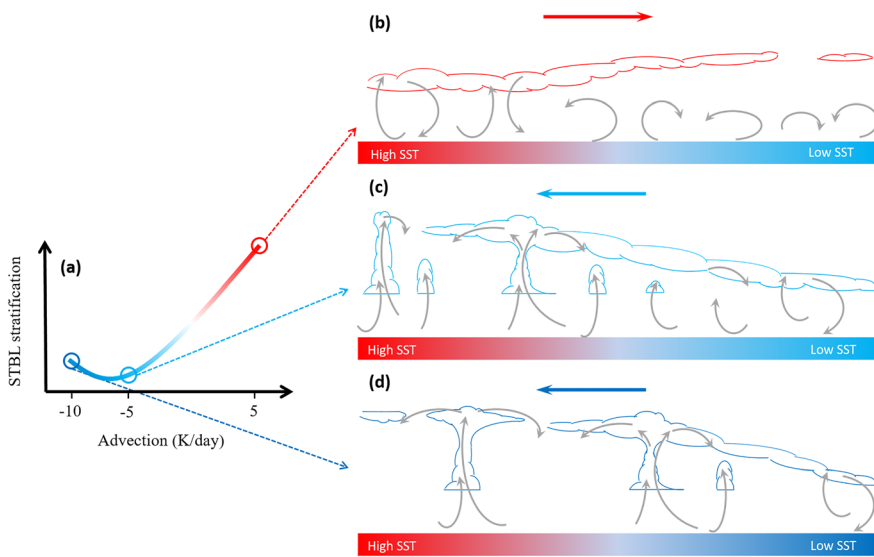
Figure 4. Cartoons illustrating how STBL coupling state responds to low-level temperature advections with different signs and strengths.

advection where stratocumulus clouds may occur. We use ground-based observations, reanalysis datasets of meteorological fields, and satellite observations collected during field campaigns over three regions: the subtropical northeast Pacific, the Southern Ocean, and the Azores Island that straddles the boundary between the midlatitude and subtropical Atlantic oceans. The data samples encompass a wide range of large-scale dynamic environments, allowing us to achieve our objectives. The major conclusions, which are illustrated in a schematic diagram of Figure 4, can be summarized as follows:

1. From warm to cold air advection, a STBL tends to become more coupled (Figures 4b and 4c). This is primarily attributed to the strong synoptic control of temperature advection on atmospheric static stability: Cold advection destabilizes the lower atmosphere, leading to the release of mean flow potential energy to enhance turbulent mixing of a STBL.

2. When cold air advection becomes very strong (in our study, $< \sim -5$ K/day), a STBL becomes more stably stratified (Figure 4d). This can be explained by the "deepening-warming" decoupling mechanism (Bretherton & Wyant, 1997): When the surface warming rate is intensified, an initially well-mixed STBL may deepen so rapidly that a thermodynamic stratification occurs much earlier, leading to a cumulus-coupled STBL during a longer period of its lifetime.

3. Even in strong cold air advection where most STBLs are stably stratified due to the "deepening-warming" decoupling, they are still considerably more coupled than STBLs in warm advection (Figure 4a). This contributes to the existing body of knowledge by revealing that STBLs in subtropical downstream oceans are only weakly decoupled and that unambiguously decoupled STBLs occur in warm advection conditions (Figure 4b). This also supports our promotion that the direction and strength of temperature advection must be more seriously considered in STBL decoupling research.

Data Availability Statement

The ground-based data in this study are available from website of ARM Climate Research Facility (www.archive.arm.gov/data). The geostationary satellite cloud products are from the NASA Langley Cloud and Radiation Research Group (satcorps.larc.nasa.gov/). The reanalysis data are obtained from European Center for Medium Range Weather Forecasts (www.ecmwf.int). The HYSPLIT model is from the NOAA Air Resources Laboratory (https://www.arl.noaa.gov/hysplit/hysplit/).

Appendix A.: Discussion of z_i Dependence on T_{adv}

According to the mixed-layer theory (Lilly, 1968), z_i is primarily dependent on two factors: the entrainment rate and the large-scale vertical velocity. As stated in the main text, in extremely cold advection conditions,

the "deepening-warming" mechanism dominates, leading to strong entrainment rate and thus large z_i. In warm advection conditions, the large-scale ascent motion is dominant according to the knowledge of classical synoptic meteorology (Holton, 1973) and Figure S3. The large-scale ascent contributes to a larger z_i. Therefore, in principle, the z_i response to T_{adv} should manifest a "V" shape, which is shown by the data from CAP-MBL and MARCUS in Figure 2b. The MAGIC data, however, exhibit an opposite trend. This can be explained by the spatial co-variation between z_i and T_{adv} in the subtropical oceans (Figure S5): Cold advection is weaker in the downstream of subtropics where the z_i is larger. Note that such a spatial co-variation does not influence our primary result of T_{adv} enhancing decoupling because the dependence of $\theta_e^{top}-\theta_e^{bot}$ on the T_{adv} for the MAGIC (Figure 2a) is much larger than what can be explained by the change in z_i.

References

Agee, E. M. (1987). Mesoscale cellular convection over the oceans. *Dynamics of Atmospheres and Oceans*, *10*(4), 317–341. https://doi.org/10.1016/0377-0265(87)90023-6

Albrecht, B. A., Randall, D. A., & Nicholls, S. (1988). Observations of marine stratocumulus clouds during FIRE. *Bulletin of the American Meteorological Society*, *69*(6), 618–626. https://doi.org/10.1175/1520-0477(1988)069<0618:OOMSCD>2.0.CO;2

Berrisford, P., Dee, D., Poli, P., Brugge, R., Fielding, K., Fuentes, M., et al. (2011). *The ERA-interim archive*, version 2.0. Shinfield Park, Reading: European Centre for Medium-Range Weather Forecasts.

Bretherton, C. S. (1997). Convection in stratocumulus-topped atmospheric boundary layers. In *The physics and parameterization of moist atmospheric convection*, (pp. 127–142). New York, NY: Springer.

Bretherton, C. S., Klinker, E., Betts, A., & Coakley, J. Jr. (1995). Comparison of ceilometer, satellite, and synoptic measurements of boundary-layer cloudiness and the ECMWF diagnostic cloud parameterization scheme during ASTEX. *Journal of the Atmospheric Sciences*, *52*(16), 2736–2751. https://doi.org/10.1175/1520-0469(1995)052<2736:COCSAS>2.0.CO;2

Bretherton, C. S., & Wyant, M. C. (1997). Moisture transport, lower-tropospheric stability, and decoupling of cloud-topped boundary layers. *Journal of the Atmospheric Sciences*, *54*(1), 148–167. https://doi.org/10.1175/1520-0469(1997)054<0148:MTLTSA>2.0.CO;2

Fletcher, J. K., Mason, S., & Jakob, C. (2016). A climatology of clouds in marine cold air outbreaks in both hemispheres. *Journal of Climate*, *29*(18), 6677–6692. https://doi.org/10.1175/JCLI-D-15-0783.1

George, R. C., & Wood, R. (2010). Subseasonal variability of low cloud radiative properties over the southeast Pacific Ocean. *Atmospheric Chemistry and Physics*, *10*(8), 4047–4063. https://doi.org/10.5194/acp-10-4047-2010

Hartmann, D. L., Ockert-Bell, M. E., & Michelsen, M. L. (1992). The effect of cloud type on Earth's energy balance: Global analysis. *Journal of Climate*, *5*(11), 1281–1304. https://doi.org/10.1175/1520-0442(1992)005<1281:TEOCTO>2.0.CO;2

Holton, J. R. (1973). An introduction to dynamic meteorology. *American Journal of Physics*, *41*(5), 752–754. https://doi.org/10.1119/1.1987371

Jones, C., Bretherton, C., & Leon, D. (2011). Coupled vs. decoupled boundary layers in VOCALS-REx. *Atmospheric Chemistry and Physics*, *11*(14), 7143–7153. https://doi.org/10.5194/acp-11-7143-2011

Kanamitsu, M. (1989). Description of the NMC global data assimilation and forecast system. *Weather and Forecasting*, *4*(3), 335–342. https://doi.org/10.1175/1520-0434(1989)004<0335:DOTNGD>2.0.CO;2

Klein, S. A. (1997). Synoptic variability of low-cloud properties and meteorological parameters in the subtropical trade wind boundary layer. *Journal of Climate*, *10*(8), 2018–2039. https://doi.org/10.1175/1520-0442(1997)010<2018:SVOLCP>2.0.CO;2

Klein, S. A., Hartmann, D. L., & Norris, J. R. (1995). On the relationships among low-cloud structure, sea surface temperature, and atmospheric circulation in the summertime northeast Pacific. *Journal of Climate*, *8*(5), 1140–1155. https://doi.org/10.1175/1520-0442(1995)008<1140:OTRALC>2.0.CO;2

Lewis, E. R. (2016). *Marine ARM GPCI Investigation of clouds (MAGIC) field campaign report (No. DOE/SC-ARM-16-057)*. Washington, DC: DOE Office of Science Atmospheric Radiation Measurement (ARM) Program.

Lilly, D. K. (1968). Models of cloud-topped mixed layers under a strong inversion. *Quarterly Journal of the Royal Meteorological Society*, *94*(401), 292–309. https://doi.org/10.1002/qj.49709440106

McCoy, I. L., Wood, R., & Fletcher, J. K. (2017). Identifying meteorological controls on open and closed mesoscale cellular convection associated with marine cold air outbreaks. *Journal of Geophysical Research: Atmospheres*, *122*, 11,678–611,702. https://doi.org/10.1002/2017JD027031

McFarquhar, G., Maarchand, R., Bretherton, C., Alexander, S., Protat, A., Siems, S., et al. (2019). Measurements of Aerosols, Radiation, and Clouds over the Southern Ocean (MARCUS) field campaign report.(*No. DOE/SC-ARM-19-008*). USA: DOE Office of Science Atmospheric Radiation Measurement (ARM) Program.

Miller, M. A., & Albrecht, B. A. (1995). Surface-based observations of mesoscale cumulus–stratocumulus interaction during ASTEX. *Journal of the Atmospheric Sciences*, *52*(16), 2809–2826. https://doi.org/10.1175/1520-0469(1995)052<2809:SBOOMC>2.0.CO;2

Minnis, P., Kratz, D. P., Coakley, J. A. Jr., King, M. D., Garber, D., Heck, P., et al. (1995). Cloud optical property retrieval (subsystem 4.3). *Clouds and the Earth's Radiant Energy System (CERES) algorithm theoretical basis document*, *3*, 135–176.

Muhlbauer, A., McCoy, I. L., & Wood, R. (2014). Climatology of stratocumulus cloud morphologies: Microphysical properties and radiative effects. *Atmospheric Chemistry and Physics*, *14*(13), 6695–6716. https://doi.org/10.5194/acp-14-6695-2014

Nicholls, S. (1984). The dynamics of stratocumulus: Aircraft observations and comparisons with a mixed layer model. *Quarterly Journal of the Royal Meteorological Society*, *110*(466), 783–820. https://doi.org/10.1002/qj.49711046603

Nicholls, S., & Leighton, J. (1986). An observational study of the structure of stratiform cloud sheets: Part I. *Structure. Quarterly Journal of the Royal Meteorological Society*, *112*(472), 431–460. https://doi.org/10.1002/qj.49711247209

Norris, J. R., & Iacobellis, S. F. (2005). North Pacific cloud feedbacks inferred from synoptic-scale dynamic and thermodynamic relationships. *Journal of Climate*, *18*(22), 4862–4878. https://doi.org/10.1175/JCLI3558.1

Norris, J. R., & Klein, S. A. (2000). Low cloud type over the ocean from surface observations. Part III: Relationship to vertical motion and the regional surface synoptic environment. *Journal of Climate*, *13*(1), 245–256. https://doi.org/10.1175/1520-0442(2000)013<0245:LCTOTO>2.0.CO;2

Parfitt, R., Czaja, A., & Seo, H. (2017). A simple diagnostic for the detection of atmospheric fronts. *Geophysical Research Letters*, *44*, 4351–4358. https://doi.org/10.1002/2017GL073662

Stein, A., Draxler, R. R., Rolph, G. D., Stunder, B. J., Cohen, M., & Ngan, F. (2015). NOAA's HYSPLIT atmospheric transport and dispersion modeling system. *Bulletin of the American Meteorological Society*, *96*(12), 2059–2077. https://doi.org/10.1175/BAMS-D-14-00110.1

Stevens, B., Cotton, W. R., Feingold, G., & Moeng, C.-H. (1998). Large-eddy simulations of strongly precipitating, shallow, stratocumulus-topped boundary layers. *Journal of the Atmospheric Sciences*, *55*(24), 3616–3638. https://doi.org/10.1175/1520-0469(1998)055<3616:LESOSP>2.0.CO;2

Wall, C. J., Hartmann, D. L., & Ma, P.-L. (2017). Instantaneous linkages between clouds and large-scale meteorology over the Southern Ocean in observations and a climate model. *Journal of Climate*, *30*(23), 9455–9474. https://doi.org/10.1175/JCLI-D-17-0156.1

Whiteman, C. D., Bian, X., & Zhong, S. (1999). Wintertime evolution of the temperature inversion in the Colorado Plateau Basin. *Journal of Applied Meteorology*, *38*(8), 1103–1117. https://doi.org/10.1175/1520-0450(1999)038<1103:WEOTTI>2.0.CO;2

Wood, R. (2012). Stratocumulus clouds. *Monthly Weather Review*, *140*(8), 2373–2423. https://doi.org/10.1175/MWR-D-11-00121.1

Wood, R., & Bretherton, C. S. (2004). Boundary layer depth, entrainment, and decoupling in the cloud-capped subtropical and tropical marine boundary layer. *Journal of Climate*, *17*(18), 3576–3588. https://doi.org/10.1175/1520-0442(2004)017<3576:BLDEAD>2.0.CO;2

Wood, R., Wyant, M., Bretherton, C. S., Rémillard, J., Kollias, P., Fletcher, J., et al. (2015). Clouds, aerosols, and precipitation in the marine boundary layer: An arm mobile facility deployment. *Bulletin of the American Meteorological Society*, *96*(3), 419–440. https://doi.org/10.1175/BAMS-D-13-00180.1

Wylie, D., Hinton, B. B., & Kloesel, K. (1989). The relationship of marine stratus clouds to wind and temperature advection. *Monthly Weather Review*, *117*(11), 2620–2625. https://doi.org/10.1175/1520-0493(1989)117<2620:TROMSC>2.0.CO;2

Xu, H., Xie, S.-P., & Wang, Y. (2005). Subseasonal variability of the southeast Pacific stratus cloud deck. *Journal of Climate*, *18*(1), 131–142. https://doi.org/10.1175/JCLI3250.1

Zheng, Y., & Li, Z. (2019). Episodes of warm-air advection causing cloud-surface decoupling during the MARCUS. *Journal of Geophysical Research: Atmospheres*, *124*, 12,227–12,243. https://doi.org/10.1029/2019JD030835

Zheng, Y., Rosenfeld, D., & Li, Z. (2016). Quantifying cloud base updraft speeds of marine stratocumulus from cloud top radiative cooling. *Geophysical Research Letters*, *43*, 11,407–11,413. https://doi.org/10.1002/2016GL071185

Zheng, Y., Rosenfeld, D., & Li, Z. (2018a). Estimating the decoupling degree of subtropical marine stratocumulus decks from satellite. *Geophysical Research Letters*, *45*, 12,560–12,568. https://doi.org/10.1029/2018GL078382

Zheng, Y., Rosenfeld, D., & Li, Z. (2018b). The relationships between cloud top radiative cooling rates, surface latent heat fluxes, and cloud-base heights in marine stratocumulus. *Journal of Geophysical Research: Atmospheres*, *123*, 11,678–611,690. https://doi.org/10.1029/2018JD028579

Zheng, Y., Rosenfeld, D., Zhu, Y., & Li, Z. (2019). Satellite-based estimation of cloud top radiative cooling rate for marine stratocumulus. *Geophysical Research Letters*, *46*, 4485–4494. https://doi.org/10.1029/2019GL082094

Zuidema, P., Painemal, D., De Szoeke, S., & Fairall, C. (2009). Stratocumulus cloud-top height estimates and their climatic implications. *Journal of Climate*, *22*(17), 4652–4666. https://doi.org/10.1175/2009JCLI2708.1